Nanoscale

Accepted Manuscript

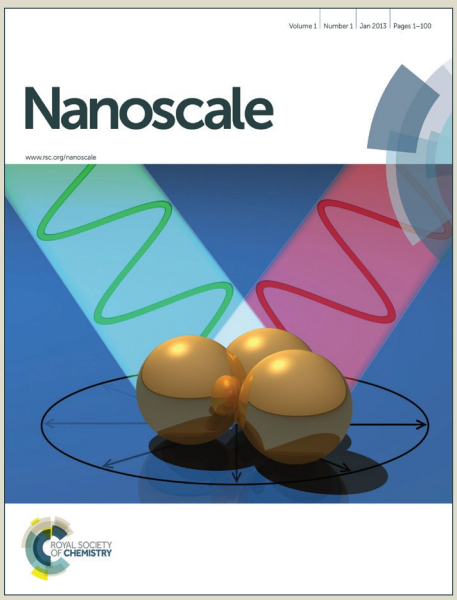

ROYAL SOCIETY OF CHEMISTRY

www.rsc.org/nanoscale

Journal Name

ARTICLE

Concentration-dependent structure and structural transition from chirality to nonchirality at the liquid-solid interface by coassembly

Li Xu,[a,b] Xinrui Miao,*[a] Lihua Cui,[a] Pei Liu,[a] XiaoFeng Chen,*[a,b] Wenli Deng*[a]

Received 00th January 20xx,
Accepted 00th January 20xx

DOI: 10.1039/x0xx00000x

www.rsc.org/

Understanding the formation and structural transition of the two-dimensional chirality of self-assembly still gained a subject of significant interest in surface or interface chirality studies. Here, we present solvent-induced chirality structural transition of 2-hydroxy-7-pentadecyloxy-9-fluorenone (HPF) molecules self-assembled adlayer through coassembly with achiral aliphatic solvents under different concentrations. Polymorphic chiral patterns are obtained at low concentrations of aliphatic solvents with different chains length. The HPF molecules form coassembled structures with these solvents through van der Waals interactions. At the same time, at high concentrations, HPF molecules uniformly form a nonchiral multimer structure without coadsorbed aliphatic solvent molecules. What is interesting is that these structures under different concentrations will finally change into a zigzag structure, which is the thermodynamically most stable configuration. Especially when using *n*-hexadecane as the solvent, the adlayer shows perfect steric matching due to the close chain length of HPF and *n*-hexadecane, which can maximize the molecule–solvent interactions. Thus, HPF molecule in *n*-hexadecane exhibits the most diversiform configuration. The distinct concentration–dependence has proven that the solvent molecules can act as a coadsorbed component through van der Waals interactions rather than simply dispersant and further result in the probability and stability of chiral self-assembled monolayers by subtle tuning the solvent–molecule and solvent–substrate interactions. This result provides a simple and alternative strategy to construct the 2D chiral assembled monolayer.

Introduction

Controlling and inducing two-dimensional chirality on solid surface has received significant attention for many years in fundamental research and potential application such as nonlinear optics, enantioselective heterogeneous catalysis, and many other important physical chemistry topics.[1-5] Understanding the two-dimensional chirality induction and amplification process, and fabricating surface chirality in surface chiral engineering is of great significance to predict and control over the 2D supramolecular chirality. Furthermore, in order to realize chiral surfaces, the formation of a chiral element can be tuned and controlled to a certain extent in the assembly process.[6-10] Meanwhile, the self-assembly of nonchiral molecules on solid surfaces has been expanded enormously, and two-dimensional (2D) chiral structures in nonchiral surface can also be achieved by exerting external stimuluses such as using chiral modifiers,[11-12] controlling temperature in the monolayer,[13] or exposing monolayer to magnetic field.[14] Except for these chiral induced methods, the solvent plays an important role as well in controlling and inducing chirality.[9, 15-23] When a chiral or achial solvent is used, this can influence on a large number of achiral molecules and assist the macroscopic chirality emergence of the monolayer in solution. For example, Katsonis *et al.* have reported that rosettes with a particular handedness were formed on the surface by using a chiral solvent. The chiral 1-phenyl-1-octanol solvent acted as supramolecular chiral regulators interacted with the hydrogen-bonding achiral diamino triazine oligo (p-phenylenevinylene) (OPV) derivatived and fabricated homochiral surfaces.[6] Although the chiral solvent molecules were not coadsorbed, hydrogen bonding interactions between hydroxy group of solvent and hydrogen bond acceptors of the OPV molecules could be considered to key role for induction of the expression of chirality at the liquid–solid interface. In addition, the coadsorption of solvent molecule through the solvent–solute noncovalent interaction also plays an important role in fabricating and manipulating chirality.[15-16, 18, 24-25] In most cases, solvent molecules will be interacted with the coadsorbed molecules in the assembly processing, such as hydrogen bonding interactions owing to their selectivity and directionality nature. For example, Wan *et al.* reported the induction of global homochirality in two-dimensional enantiomorphous networks of achiral molecules with coabsorbed chiral solvent *via* supramolecular hydrogen bonding interactions.[26] Large studies of the resulting monolayers revealed that the driving forces for the formation of chirality building block is crucially derived from selective and directional hydrogen bonding between the solute and solvent during the formation of chiral assembly processing. So far, it is still a great challenge to the detailed understanding of the underlying

[a] College of Materials Science and Engineering, South China University of Technology, Guangzhou 510640, China. E-mail: msxrmiao@scut.edu.cn, wldeng@scut.edu.cn; Tel: 86-20-22236708
[b] National Engineering Research Centre for Tissue Restoration and Reconstruction, Guangzhou, 510006, China. E-mail: chenxf@scut.edu.cn; Tel: +86-20-22236283
† Electronic Supplementary Information (ESI) available: Detailed description of experimental section and additional STM images. See DOI: 10.1039/x0xx00000x

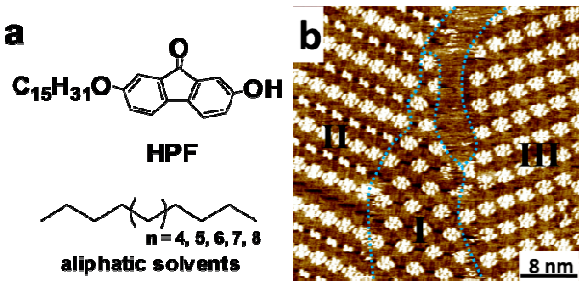

Fig.1 (a) Chemical structures of 2-hydroxy-7-(pentadecyloxy)-9-fluorenone (HPF) and aliphatic solvents (including n-hexadecane, *n*-pentadecane, *n*-tetradecane, *n*-tridecane and *n*-dodecane); (b) Large-scale STM image of HPF self-assembled monolayer at the concentrations of 3.5×10^{-7} ~ 2.5×10^{-6} mol L^{-1} in *n*-hexadecane solution on the HOPG surface shows the coexistence of three kinds of chiral patterns. Three different patterns (racemic hexamer, alternate pattern, and linear hexamer structure) are labeled as I, II, and III. Tunneling parameters: I_t = 456 pA, V_b = 655 mV.

formation mechanism of chiral assemblies, which is of great importance to steer the assembly process of fabricate potential chical assembled nanostructures. The supramolecular chiral nanostructures, on the other hand, constructed *via* molecule-solvent van der Waals (vdWs) interactions on two-dimensional achiral surfaces have seldom been reported. Therefore, we focus on understanding the underlying driving force for the chiral formation, amplification, transition, and control through the solute-solvent vdWs interactions.

Previously, we have studied the self-assembly of 2-hydroxy-7-(*n*-alkoxy)-9-fluorenone at the 1-phenyloctane/graphite interface which was constructed polymorphic structure.[27] The fluorenone derivatives with a well-defined chemical structure and complex intermolecular interactions could benefit in the formation of polymorphic structure. In the present paper, we choose 2-hydroxy-7-pentadecyloxy-9-fluorenone (HPF) molecule (Fig. 1a) to construct the polymorphic chiral nanostructures on HOPG surfaces *via* molecule–solvent vdWs interactions by choosing suitable solvent such as aliphatic solvents. *N*-hexadecane, *n*-pentadecane, *n*-tetradecane, *n*-tridecane and *n*-dodecane can be used as solvents due to different dissolubility and adsorption capacity. STM experiments revealed that by selecting aliphatic solvents with different chain-length and tuning the concentration, the structural transition from chiral loose-packing to nonchiral close-packing pattern was observed by the molecule–solvent coassembly. Due to the flexible alkyl chains of HPF molecules, the aliphatic solvents molecules as solvent filled in the gap of the side chains lamellae. The HPF molecules with coadsorbed aliphatic molecules form several unique chiral structures *via* vdWs interactions in low concentrations. However, these chiral nanostructures do not occur at high concentrations. Due to steric matching and concentration effect, the closer the size of solvents to the alkoxy chain length of HPF, the easier for the molecular arrangement to exhibit the structural diversity. The self-assembled monolayer of HPF in *n*-hexadecane could form the most diversiform configuration. What is interesting is that these structures will finally convert into a zigzag

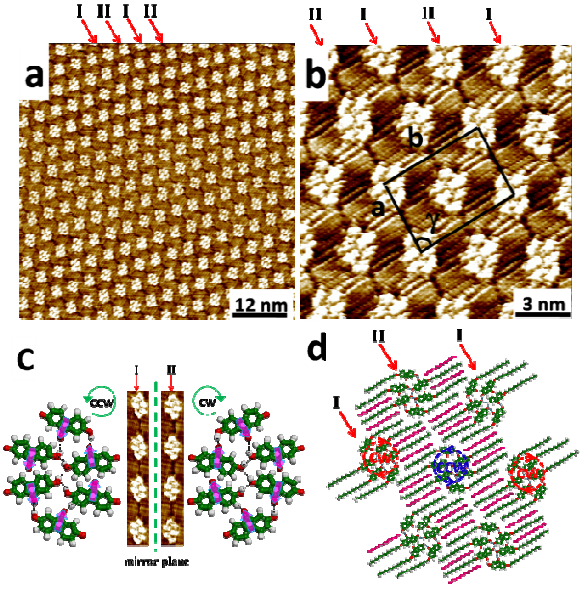

Fig. 2 (a) Large-scale STM image of the racemic hexamer for HPF self-assembled monolayer in *n*-hexadecane on HOPG surface under low concentrations; (b) High-resolution STM image of HPF self-assembled monolayer showing the arrangement of hexamer pattern. Tunneling parameters: I_t = 468 pA, V_b = 687 mV; (c) Magnified images of the mirror fluorenone units and their schematic drawings. The arrows with pink color indicate the dipole direction of conjugated groups. The green circle arrows indicate the racemic hexamer patterns of clockwise (CW) and counterclockwise (CCW) according to the dipole direction of the fluorenone units; (d) Proposed assembly model for racemic hexamer pattern..

structure, which was the thermodynamically most stable configuration. These results can better promote our understanding the molecule–solvent noncovalent interactions which dominate the surface chiral structure and provide a new strategy on efficient fabrication and control of the chiral polymorphisms in 2D assemblies.

Results

Concentration-Dependent Multiple Chiral Structural Transition in the *n*-Hexadecane Solvent

First of all, we investigated the self-assembly of HPF at the *n*-hexadecane solution/HOPG interface under low concentrations (3.0×10^{-7} ~ 2.5×10^{-6} mol L^{-1}). Unexpectedly, the STM images revealed that the HPF molecules form three kinds of chiral patterns: racemic hexamer, alternate pattern, and linear hexamer. The large-scale STM image of the polymorphic structure with three different domains (marked as I, II and III) with strikingly different contrasts and symmetries are shown in Fig. 1b.

Fig. 2a shows a representative large-scale STM image of the hexamer of HPF molecules on HOPG surface under ambient conditions. It is clear that a well-defined ordered pattern is formed, which consists of bright rods. Careful observations show that the bright rods consisted of six fluorenone cores of HPF molecules form the hexamer pattern. Moreover, there are two different hexamer

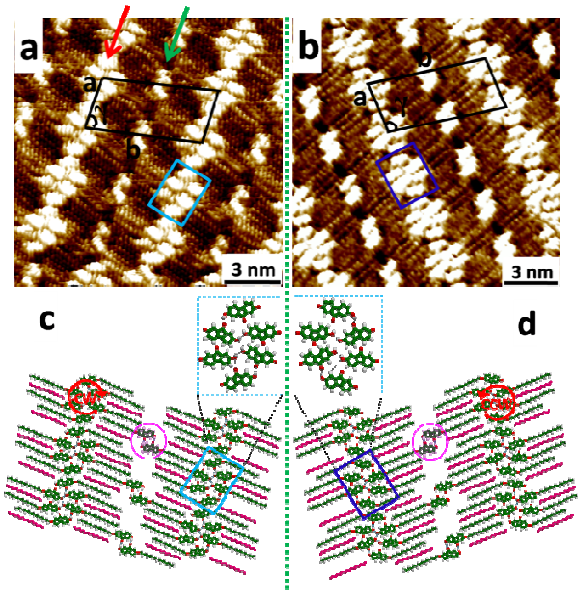

Fig. 3 High-resolution STM images of the homochiral alternate pattern of HPF in the *n*-hexadecane under low concentrations with (a) CW pattern and (b) CCW pattern. Tunneling parameters: (a) I_t = 465 pA, V_b = 755 mV; (b) I_t = 485 pA, V_b= 805 mV. (c, d) Proposed models for alternate pattern with CW and CCW structures. The red open–circle arrows indicate the opposite rotation direction of the alternate pattern in building unit. The enlarged inset in (c) and (d) shows the possible optimized hydrogen bonds with alternate architectures with CW and CCW, respectively.

patterns (marked I and II) in the adlayer, which are arranged alternately. The high-resolution STM image (Fig. 2b) of the HPF self-assembled monolayer manifests the more detailed packed pattern of hexamer, which is the essential subunit of the adlayer and a lamellar arrangement. The unit cell parameters of Fig. 2b can be defined as a = 4.4 ± 0.1 nm, b = 6.0 ± 0.1 nm, and γ = 83 ± 2°. The molecular density is 2.2 nm^2 per molecule. The combined pink arrows in Fig. 2c show the relative orientation of the carbonyl in the fluorenone unit. Six HPF molecules in turn form the enantiotopic hexamer structure according to the stretching direction of the carbonyl in the fluorenone unit. Furthermore, each lamella is comprised of hexamers with the same rotating direction. Adjacent lamellar pattern possesses opposite rotary direction, suggesting mirror image symmetry. We identify the hexamer structure as clockwise (CW) and counterclockwise (CCW), in accordance with the dipole direction of the fluorenone units. These enantiomorphous lamellae (lamellae I and lamellae II) arrange alternately on the HOPG surface and produce a racemic hexamer pattern. Careful inspections of chiral structure, it is found that bright rods align parallelly to fill with neighboring alkoxy side chains (Fig. S1†). The length and the shape of excess alkyl chains are attributed to the coadsorption of *n*-hexadecane molecules indicated in pink stripes in Fig. 2d. The stability of these coadsorbed patterns result from the perfect interdigitation between the alkoxy chains of HPF and *n*-hexadecane molecules by the vdWs interactions. According to the molecular arrangement and chirality, a structural model is proposed in Fig. 2d for the racemic assembly. The red and blue circle arrows indicate the opposite rotation direction of hexamer pattern in building units on the HOPG surface. The HPF molecules entirely form enantiomorphic hexamer fashion.

Previous studies had shown that a strong interaction among the fluorenone moieties resulted from their strong polarity.[27-30] In the structural model (Fig. 2c), six HPF molecules in one hexamer unit present combined cycle dipoles, which can maximize dipolar interactions and result in the lowest energy. Simultaneously, the six HPF molecules interact through intermolecular hydrogen bonding in head-to-head and head-to-middle fashions and form four –OH···O– hydrogen bonds and two –OH···O= hydrogen bonds. Due to the high selectivity and directionality of hydrogen bonding, HPF molecules arrange into asymmetry six-petalled shape patterns. Moreover, the alkoxy side chains of HPF keep their interdigitation arrangement and lie flat on the surface with the coadsorbed *n*-hexadecane molecules through vdWs interactions. The intermolecular hydrogen bonding, vdWs interactions and dipole–dipole interactions contribute to the probability and stability of the racemic structure.

Another chiral alternate pattern of the HPF self-assembled monolayer is shown in Fig. 3. Fig. 3a, b show the detailed packed pattern of the homochiral alternate structure. The domain size for the alternate pattern is relatively small (Fig. S2a†). Unlike the racemic hexamer pattern, the chiral alternate pattern indicated by red and green arrows apparently consists of close-packed hexamer and dimer patterns alternately (Fig. 3a). In the hexamer pattern (as indicated by azure rectangle), six molecules in turn form the CW hexamer structure according to the orientation and dipole direction of the carbonyl in the fluorenone unit, which is similar to the racemic hexamer pattern in Fig. 2. In another row, two neighboring molecules form a dimer through two –OH···O= hydrogen bonds with a back-to-back configuration (as marked by pink circles in Fig. 3c, d) and arrange with adjacent hexamers. Alkoxy side chains in adjacent rows of the close-packed hexamer and the dimer adsorb on the surface and interdigitate with each other. The high-resolution STM image clearly displays that the *n*-hexadecane molecules fill in the gap between adjacent rows as the red arrows indicated in Fig. S2b† and take part in the assembly formation. Fig. 3b shows opposite rotating direction of CCW alternate fashion. Two mirror alternate patterns possess opposite handedness and form homochiral structures. The unit cell parameters can be measured as a = 2.9 ± 0.2 nm, b = 6.7 ± 0.2 nm, γ = 73 ± 1° for CW alternate pattern, and a = 2.9 ± 0.1 nm, b = 6.6 ± 0.1 nm, γ = 74 ± 1° for CCW alternate pattern in Fig. 3b and 3c, respectively. The molecular densities are about 2.3 nm^2 per molecule for CW and CCW patterns, almost equal to those of racemic hexamer pattern. Therefore, from the STM observations, the hexamer and alternate pattern were always coexist at the same time. For the sake of clarity, structural models for the chiral alternate pattern are proposed in Fig. 3c, d. The enlarged insets in Fig. 3c and 3d provide the possible –OH···O– and –OH···O= hydrogen bonds in the hexamer lamellae shown by dashed lines, which are the same as that of racemic hexamer pattern. Similar to racemic hexamer pattern, all of the alkoxy chains in the alternate pattern keep their interdigitated arrangements with the adsorbed *n*-hexadecane solvents and lie flat on the surface, which demonstrates that the strength of the vdWs interactions are almost the same in the self-assembly process. However, the intermolecular hydrogen bonding existing in the

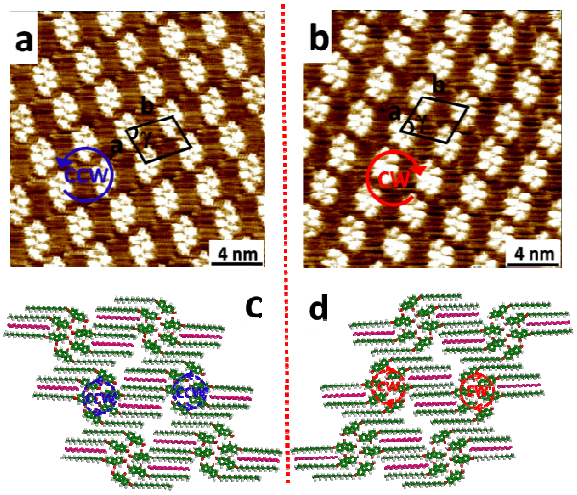

Fig. 4 High-resolution STM images of the homochiral linear hexamer of HPF in the *n*-hexadecane under low concentrations with (a) CCW pattern and (b) CW pattern. Tunneling parameters: I_t = 497 pA, V_b = 785 mV. The blue and red open-circle arrows indicate the homochiral linear hexamer architectures of CCW and CW according to the dipole direction of the fluorenone units. (c) Proposed models for linear hexamer with CCW and CW structure, respectively. The blue and red circle arrows indicate the opposite rotation direction of the homochiral linear hexamer in building unit.

dimer lamellae of alternate pattern results in important morphological changes.

In addition to racemic hexamer and alternate patterns, one new structure was also obtained (see Fig. 1) in *n*-hexadecane under low concentrations as revealed in Fig. 4a, b, which was always coexisted with other two patterns. From high-resolution images of the new structure, a homochiral linear hexamer pattern can be identified, which is similar to the close-packed hexamer lamellae in the alternate pattern. The linear hexamer structures with opposite propagation direction according to the dipole orientation and direction of the fluorenone units appeared mirror image symmetry. Comparing with the racemic hexamer structure, which possesses opposite handedness between adjacent lamellar patterns, the linear hexamer structure is comprised of hexamer with the same rotating direction. By counting the number of the chains and the side chains of HPF, we conclude that the *n*-hexadecane molecules can occupy the space between the alkoxy chains of HPF and coadsorb on the HPOG surface. The unit cell parameters of chiral hexamer structures are a = 2.9 ± 0.1 nm, b = 3.6 ± 0.1 nm, γ = 81 ± 1° for CCW hexamer, and a = 2.9 ± 0.1 nm, b = 3.6 ± 0.1 nm, γ = 80 ± 1° for CW hexamer. Based on the above analysis, the corresponding molecular models are tentatively proposed as shown in Fig. 4c, d for CCW and CW linear hexamer structures. The molecular densities are about 1.7 nm^2 per molecule for CW and CCW patterns, which are larger than two other structures. During the scanning process for each pattern, no obvious structural transition was found. Three kinds of chiral structures were in relatively stable state. In STM experiments, the total areas of the three chiral well-organized structures grow larger along with continuous scanning in same regions (Fig. S3†). Initially, three different kinds of chiral patterns

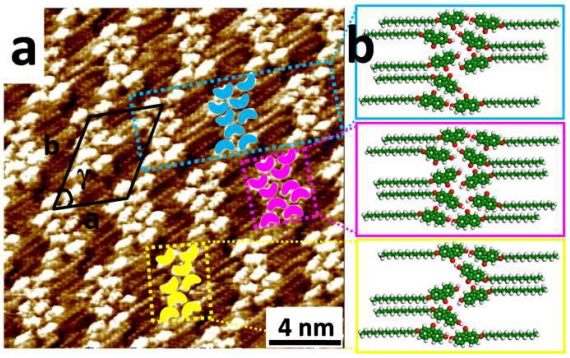

Fig.5 (a) Representative STM image of HPF adlayer showing the achiral multimer structure with three elementary structural units (8-, 9-, and 10-fold rings). The yellow, blue, and pink dashed rectangles indicate three kinds of multimer structures. Tunneling parameters: I_t = 435 pA, V_b = 695 mV. (b) Molecular models for three elementary structural units.

were observed in blurred regions, which are probably regions of high mobility that will result in lower resolution during imaging. However, following consecutive scanning, the whole surface became covered distinctly by three kinds of chiral patterns, because a solute molecule was energetically more stable on the surface than in solution.[31] Ultimately, HPF molecules are completely covered with the graphite surface for process, which is favorable for an energy minimization.

With further research, a nonchiral close-packing structure could be obtained by increasing the HPF concentration (1.0×10^{-5} ~ 2.5×10^{-5} mol L^{-1}). Fig. 5a is a representative high-resolution STM image of the most commonly observed one. The denser multimer structure with three elementary structural units (8-, 9-, and 10-fold rings) are clearly displayed. As shown in the STM image, eight, nine or ten HPF molecules congregate in back-to-abdomen and form a multimer configuration, which is the basic unit of the adlayer. To illustrate the multimer configuration clearly, three schematic multimer configurations (labeled by different colored kidney) are superimposed on Fig. 5a. Nevertheless, the arrangements of the octamer, nonamer and decamer are random. No more than three continuous octamers or decamers are observed in the STM images. The nonamer structure is the most common one denoted by the blue dashed rectangle in Fig. 5a and S4†. The molecular density is about 1.3 nm^2 per molecule. On the basis of the above analysis, structural models about three kinds of multimer structures are tentatively proposed in Fig. 5b.

The expressing of chirality was influenced by tuning the concentration. With the increase of HPF concentration, the solute may adsorb on the surface more efficiently, resulting in the change of molecule–molecule, solvent–molecule, and solvent–substrate interactions, thus inducing a new structure on the same substrate. The large-scale STM image (Fig. S5†) also reveal that these three chiral well-organized structures gradually transform into nonchiral multimer structure by consecutive scanning for more than two hours. Since the STM experiments were carried out in open environment, the evaporation of *n*-hexadecane was unavoidable. Thus the solute concentration must increase

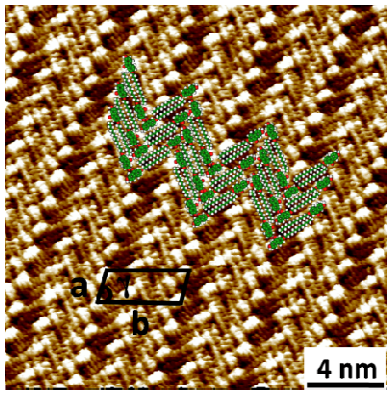

Fig. 6 High-resolution STM image of the zigzag structure. Schematic representation of HPF is superimposed on the image to clarify the molecular arrangement. Tunneling parameters: I_t = 485 pA, V_b = 675 mV.

concomitantly for a long time of the scanning process. This phenomenon reflects the sensitivity of the system toward changes in the concentration due to the solvent evaporation.

Similar to the assembled structure of HPF molecule in 1-phenloctane,[27] all the different structures of the HPF adlayers would ultimately convert into the most stable zigzag conformation after being scanned for a period of times. The high-resolution image (Fig. 6) shows that the conjugated moiety of the HPF molecule interacts with those of neighboring molecules through sequential –OH···O= hydrogen bonds as the superimposed molecular model shown in Fig. 6. The HPF molecules form continuous hydrogen bonds and arrange in a zigzag fashion. Similarly, the chiral arrangement was not observed in the zigzag pattern. Based on an energy minimization of this configuration, the most stable zigzag conformation was found to adopt the closest-packed structure, which was favorable in terms of enthalpy.[32-33] The unit cell parameters are measured as a = 3.9 ± 0.1 nm, b = 1.3 ± 0.1 nm, and γ = 86 ± 1°. The molecular density is about 1.26 nm^2 per molecule, which is the highest packing density in all of the structures. The result suggests that molecules with different conformations have different contact areas with the surfaces, leading to a difference in adsorption energy, and in turn to preferential adsorption.[34] In view of the total system energy, densely packed assembly is most frequently favored in which the molecule–substrate and molecule–molecule interactions could be maximized, especially when the intermolecular interaction lacks directionality.[35]

Self-assembled structure of HPF in other aliphatic solvents

To gain further insight into the solvent and concentration effects on the self-assembly of HPF, the self-assembly of HPF monolayers in different alkane solvents were also investigated. A droplet of HPF solution in *n*-pentadecane was applied onto the substrate with the solution concentration of 4.0 × 10^{-7} ~ 1.2 × 10^{-6} mol L^{-1}, the close-packed hexamer with opposite propagation direction can be clearly viewed in Fig. 7a, which exhibit enantiomer domains and denote with CW and CCW by irregular borderlines. Fig. 7b and 7c are the high-resolution STM images, showing the details of the 2D chiral close-packed hexamer structure with mirror image symmetry.

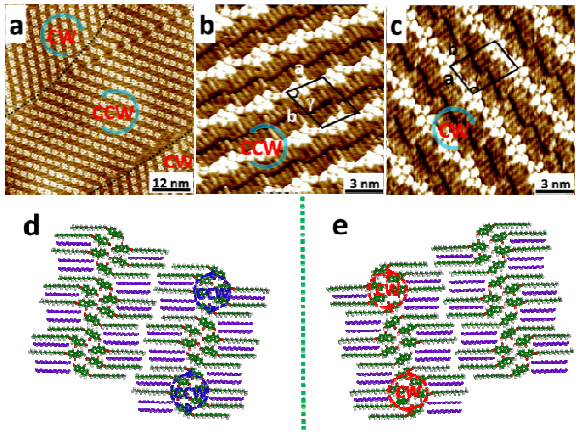

Fig. 7 (a) Large-scale STM image of the close-packed hexamer architecture of HPF in *n*-pentadecane with the solution concentrations from 4.0 × 10^{-7} mol L^{-1} to 1.2 × 10^{-6} mol L^{-1}. Tunneling parameters: I_t = 455 pA, V_b = 690 mV. The blue open-circle arrows indicate the close-packed hexamer architectures of CW and CCW according to the orientation and dipole direction of the fluorenone units, respectively. The black dashed line separates a CW and a CCW hexamer domain. (b) High-resolution STM image for CCW close-packing hexamer pattern: I_t = 585 pA, V_b = 775 mV. (c) CW close-packed hexamer pattern: I_t = 485 pA, V_b = 782 mV. (d) Proposed models for close-packed hexamer architectures with CCW and CW. The blue circle arrows indicate the opposite rotation direction of the close-packed hexamer architectures in building unit.

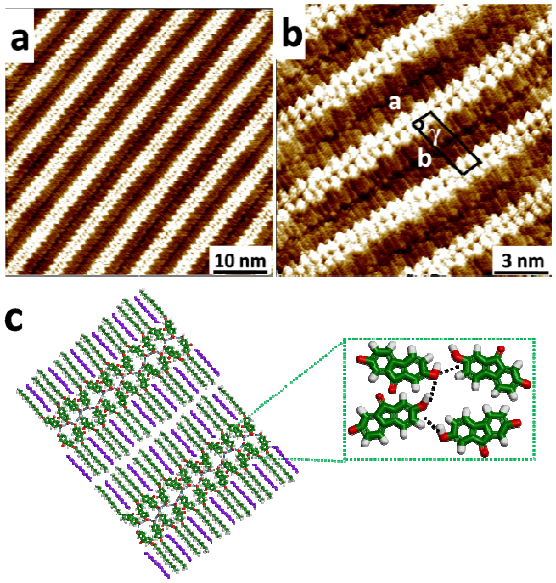

Fig. 8 (a, b) Large-scale and high-resolution STM images of the linear pattern in *n*-pentadecane (1.5 × 10^{-6} ~ 4.0 × 10^{-6} mol L^{-1}) on HOPG surface. Tunneling parameters: I_t = 445 pA, V_b = 645 mV. (c) Proposed model for the linear pattern. The enlarged inset indicates the possible optimized hydrogen bonds.

Comparing with the alternate pattern in *n*-hexadecane, the chiral close-packed hexamer structure in *n*-pentadecane is the same with the close-packed hexamer lamellae in the alternate pattern. Six

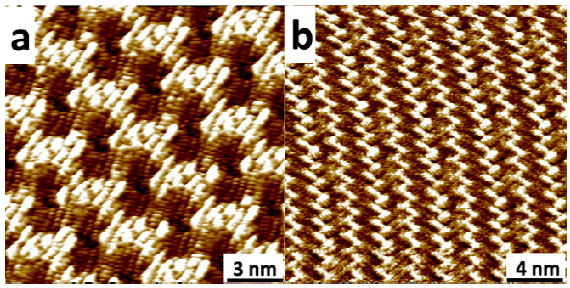

Fig. 9 (a) High-resolution STM image of HPF shows the multimer structure on HOPG surface in *n*-pentadecane at high concentration (4.0×10^{-6} ~ 1.5×10^{-5} mol L^{-1}). Tunneling parameters: I_t = 565 A, V_b = 725 mV. (b) High-resolution STM image showing a zigzag pattern of HPF. Tunneling parameters: I_t = 554 pA, V_b = 665 mV.

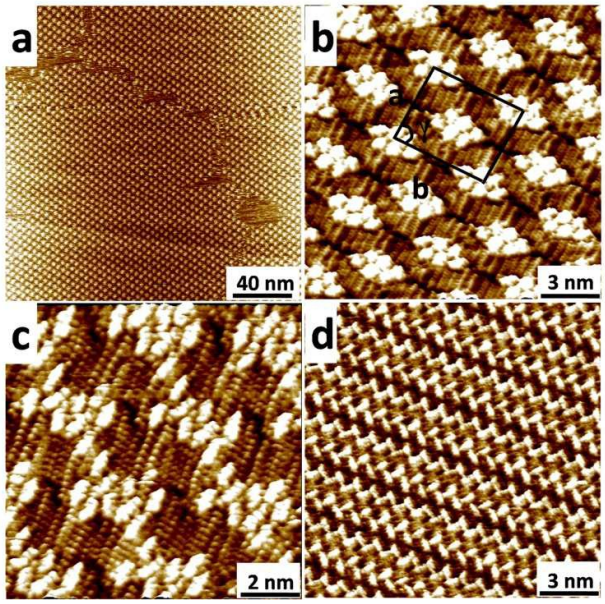

Fig. 10 (a, b) Large-scale and high-resolution STM images of racemic hexamer pattern in *n*-tetradecane with a low concentration on HOPG surface. Tunneling parameters: I_t = 535 pA, V_b = 605 mV. (c) High-resolution STM image of HPF shows the multimer structures with three elementary structural unit (8-, 9-, and 10-fold rings) in *n*-tetradecane on HOPG surface at a high concentration. Tunneling parameters: I_t = 479 pA, V_b = 612 mV. (d) High-resolution STM image showing a zigzag pattern of HPF. Tunneling parameters: I_t = 433 pA, V_b = 625 mV.

molecules in turn form the homochiral hexamer structure according to the orientation and dipole direction of the fluorenone units. The side chains in adjacent rows stack in a tail-to-tail fashion. Since the alkoxy side chains in adjacent rows cannot form close-packed structure, which was not in favor of the vdWs interactions. Similarly, the *n*-pentadecane molecules fill in the arrangement space of neighboring side chains. The amount of coadsorbed solvents is important for the formation of chiral pattern and enhances the adlayer stability through vdWs interactions. Based on above analysis, the corresponding molecular models are tentatively proposed in Fig. 7d and 7e for CW and CCW chiral assemblies. The unit cell parameters are a = 2.8 ± 0.1 nm, b = 4.4± 0.1 nm, γ = 65 ± 1° for CCW hexamer, and a = 2.9 ± 0.2 nm, b = 4.2 ± 0.2 nm, γ = 64 ± 2° for CW hexamer in Fig. 7b and 7c, respectively.

When the HPF concentration increases to 1.5×10^{-6} ~ 4.0×10^{-6} mol L^{-1}, the close-packed hexamer pattern disappeared gradually and a linear pattern was observed (Fig. 8a). The structural details are revealed by a high-resolution STM image shown in Fig. 8b. Four HPF molecules pack in a head-to-head fashion *via* sequential –OH···O– hydrogen bonds and form a tetramer as the basic unit of the adlayer. The side chains in adjacent lamellae arrange in a tail-to-tail fashion. Solvent molecules coadsorb with HPF molecules due to the space matching. We propose the molecular packing model in Fig. 8c. The unit cell parameters of linear structures are a = 0.8 ± 0.1 nm, b = 5.6 ± 0.1 nm, and γ = 84 ± 1°.

Similar to the HPF self-assembled adlayer in *n*-hexadecane, the multimer structure with three elementary structural units (8-, 9-, and 10-fold rings) can also be discerned with further increase of the concentrations (Fig. 9a). Moreover, as the extension of scanning time, the homochiral close-packed hexamer and linear patterns gradually transformed into multimer structure (Fig. S6 and S7†). Finally, after being scanned for a period of time, the multimer layer was also converted into the zigzag structure step by step (Fig. 9b). The results further demonstrate that the zigzag pattern is the most stable architecture considering the total gain in the energy of the system.[27]

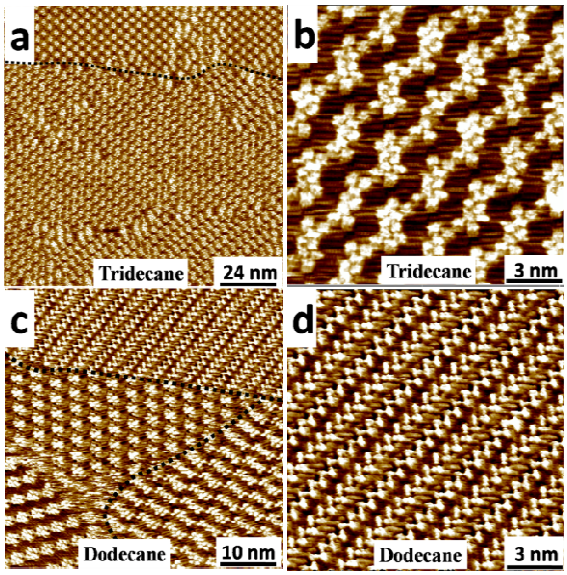

Fig. 11 (a) Large-scale STM image of the HPF self-assembled monolayer in *n*-tridecane on HOPG surface. Tunneling parameters: I_t = 503 pA, V_b = 658 mV. (b) High-resolution STM image of the multimer pattern in *n*-tridecane. Tunneling parameters: I_t = 564 pA, V_b = 597 mV. (c) STM image of three kinds of arrangements in *n*-dodecane on HOPG surface. Tunneling parameters: I_t = 516 pA, V_b = 624 mV. (d) High-resolution STM image of the zigzag structure in *n*-dodecane. Tunneling parameters: I_t = 526 pA, V_b = 675 mV.

Table 1 Unit Cell Parameters and Other Characteristic Parameters of Monolayers of HPF in Different Aliphatic Solvents under Different Concentrations.

Slovent	Pattern	Unit cell parameters			No. of molecules per unit	Unit cell area(nm^2)	Unit cell area (nm^2)/N_m
		a (nm)	b (nm)	γ (°)	N_m[a]	S[a]	S_n[a]
n-hexadecane	Racemic hexamer	4.4 ± 0.1	6.0 ± 0.1	83 ± 2	12	26.1	2.2
	Alternate[b]	2.9 ± 0.2	6.7 ± 0.2	73 ± 1	8	18.6	2.3
	Linear hexamer[b]	2.9 ± 0.1	3.6 ± 0.1	80 ± 1	6	10.3	1.7
	Multimer[c]	-	-	-	-	-	1.3
n-pentadecane	Close-packed hexamer[b]	2.9 ± 0.2	4.2 ± 0.2	64 ± 2	6	10.9	1.8
	Linear	0.8 ± 0.1	5.6 ± 0.1	84 ± 1	4	4.6	1.2
	Multimer[c]	-	-	-	-	-	1.3
n-tatredecane	Racemic hexamer	4.3 ± 0.1	6.0 ± 0.1	82 ± 1	12	25.5	2.1
	Multimer[c]	-	-	-	-	-	1.3
n-tridecane[d]	Linear hexamer	-	-	-	-	-	-
	Multimer[c]	-	-	-	-	-	1.3
n-dodecane[e]	Linear hexamer	-	-		-	-	-
	Multimer[c]	-	-	-	-	-	-

[a] N_m = number of molecules per unit cell. S = unit cell area (nm^2). S_m = unit cell area divided by number of molecules per unit cell area. [b] Unit cell parameters are determined as CW pattern. [c] Multimer pattern is uncertain about unit cell parameters. [d] Unit cell parameters are not determined due to unstable racemic hexamer pattern in *n*-tridecane. [e] Unit cell parameters are not determined due to unstable liner hexamer and multimer pattern in *n*-dodecane.

When *n*-tetradecane was used as the solvent, a racemic hexamer pattern was obtained exclusively on a larger scale under low concentrations ($1.5 \times 10^{-6} \sim 1.0 \times 10^{-5}$ mol L^{-1}) (Fig. 10a). As shown in Fig. 10b, the racemic hexamer pattern is similar to the HPF self-assembled structures in *n*-hexadecane solvent under low concentrations. No other structures are observed at low concentrations. The multimer structure, which is similar to that in *n*-hexadecane solvent, was observed at high concentrations ($5.0 \times 10^{-6} \sim 2.0 \times 10^{-5}$ mol L^{-1}) as shown in Fig. 10c. In the same way, as the extension of scanning time, the multimer pattern can completely transform into the zigzag pattern. Finally, the whole scanning area is covered by the zigzag structure as shown in Fig. 10d and S8†.

After studying the monolayers of HPF molecule on HOPG surfaces in *n*-tridecane and *n*-dodecane, the self-assembled adlayer of HPF was further investigated to illustrate the solvent effect on molecular assembly on the surfaces. Fig. 11a is the large-scale STM image of HPF adlayer on the HOPG surface using *n*-tridecane as the solvent. The well-ordered adlayer with racemic hexamer pattern and multimer pattern could be observed. Owing to its instability, high-resolution images of hexamer pattern could not be easily obtained in *n*-tridecane solvent. The racemic hexamer pattern could change into the multimer pattern in no time as shown in Fig. 11b. The zigzag structure covered the scanning area within a short period of time (Fig. S9†).

Three kinds of arrangements, which are the close-packed hexamer pattern, multimer pattern and zigzag pattern, could be observed using *n*-dodecane as the solvent (Fig. 11c). Compared to the self-assembly process of HPF molecule in *n*-tridecane solvent, the close-packed hexamer pattern and multimer pattern are more unstable in *n*-dodecane and completely replaced by the zigzag structure in a shorter period of time (Fig. 11c and S10†).

Discussion

Table 1 summarizes the geometric characteristics, self-assembled patterns and unit cell parameters of the physisorbed adlayers of HPF in different aliphatic solvents/graphite interfaces under different concentrations.

Structural Evolution: Coadsorbed Solvent Effect on Chiral Emergence

In self-assembly process, weak intermolecular interactions would have dramatic influence on molecular adsorption configuration and cluster in the monolayers. For chiral structure, the change of the weak interactions may drive chiral phase transition.[36-37] The solvent can have a significant effect on the

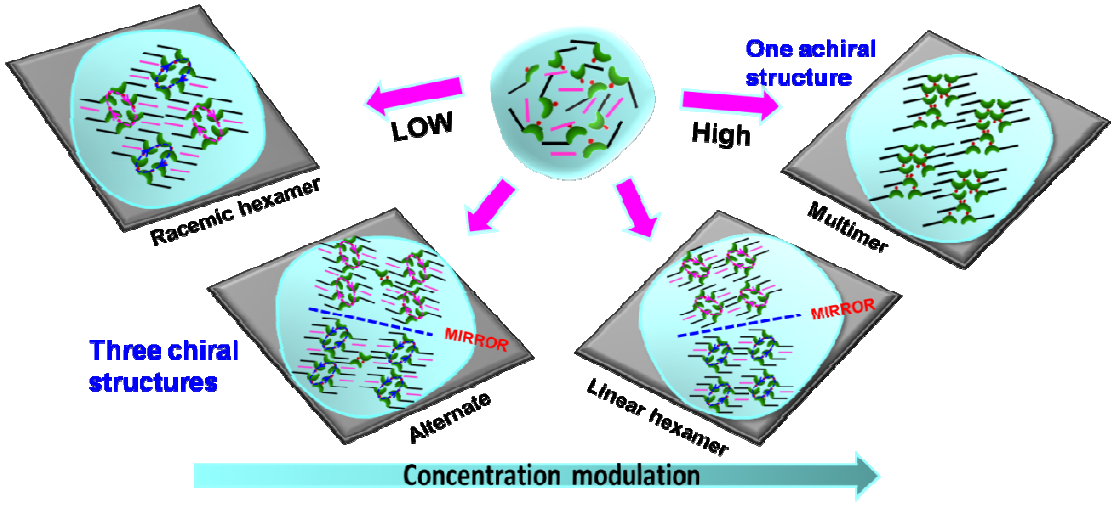

Fig. 12 Schematic representation for co-adsorption induced structural transformation from chiral loose packing to achiral close-packed pattern by concentration modulation. The light-green crescent-shaped indicates the fluorenone motifs, the black rods are the alkyl chains, and the coadsorbed aliphatic solvent molecules are indicated in peach.

expressing of chirality by tuning of intermolecular interactions between the coadsorbed molecules.[19] In the present system, by changing the solvent and tuning the solution concentration, structural transition from chiral loose-packing structures to a nonchiral close-packing pattern was obtained at the liquid–solid interface. The HPF molecules and coadsorbed aliphatic solvent molecules formed several unique chiral structures through vdWs interactions at low concentrations, whereas this chiral phenomenon did not occur at high concentrations. To better understand chiral evolution process, a corresponding schematic representation is tentatively proposed according the observed STM images. From these chiral structural models in Fig. 12, it can be clearly seen that the aliphatic solvents coadsorb with HPF molecules in the self-assembled monolayers under low concentrations. Three chiral structures can be formed through the molecule–solvent noncovalent interaction. Taking steric hindrance into account, aliphatic solvent can be coadsorbed on the graphite surface with HPF molecules, which strengthen the vdWs interactions, better stabilize the coadsorbed lamellae, and induce the formation of chiral structures. With increasing solution concentration, the solvent molecules were not coadsorbed in the multimer pattern. Solute molecules easily form a more close-packed arrangement (see Table 1) to minimize the Gibbs free energy and maximize the substrate coverage.[34-35] Without the aliphatic solvent coadsorption, nonpolar solvents are hard to modulate the formation of HPF assembled patterns. So HPF molecules form nonchiral multimer pattern according to the close-packed principle. As a result, various configurations of the self-assembled HPF molecules on HOPG surface were constructed through regulating different solution concentrations. Moreover, the formation and transition of chirality can be conducted by changing the solution concentrations and codependent molecule–solvent interactions. As a matter of fact, in addition to molecule–solvent interactions, it can also be related to solvation processes and steric restrictions within the monolayer, in which a particular assembling favored. The handedness of phase transformation under different concentrations of the HPF molecule can be explained by delicate balance among the vdWs interactions resulted from interdigitated alkyl chains of molecules, the hydrogen bonding, the dipole–dipole interactions of the fluorenone units, and the molecule–substrate interactions.

Induced Racemic Pattern Mechanism

A question arises as to why HPF molecules form the racemic pattern in *n*-hexadecane at low concentrations, where the hexamers in adjacent lamellae possesses opposite handedness. To understand the induced racemic pattern mechanism, we established a rational hypothesis regarding the molecular arrangement. We applied MS to build assembled models composed of four hexamer units. The possible formations of hexamer pattern schematically illustrated in Fig. 13b–d display all the possible interdigititated models of the adjacent hexamer units containing CW or CCW pattern. In comparison to the hexamer model in the direction of rotation (Fig. 13b), the hexamer model in the opposite direction of rotation (Fig.13c) formed a denser structure between the adjacent hexamer units. Considering the influence of the underlying substrate lattice and steric constraint, the racemic hexamer pattern adopts the much closer-packing fashion relative to the former. In other words, the racemic hexamer structure results in minimizing free energy and maximizing the substrate coverage, and therefore achieving the most stable configuration. Similarly, the formation of hexamer pattern in Fig. 13d cannot lead to a minimum in free surface area, either, because of the unfavorable interaction. These results indicate that the CW and CCW hexamer units are much more stable than the pure CW hexamer units or CCW hexamer units and explain why the CW and CCW enantiomeric hexamer units are formed selectively.

Effect of Alkyl Chain Length of Solvent

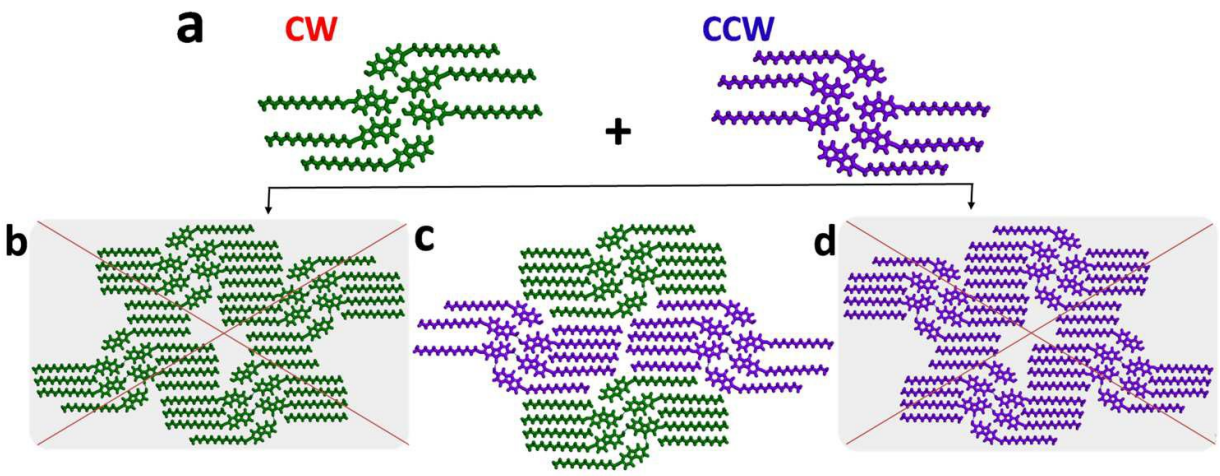

Fig. 13 Illustration of the racemic assembled formation. (a) Hexamer units as CW and CCW indicate in green and purple colors, according to the stretching direction of the carbonyl in the fluorenone unit. (b–d) Possible molecular models for the hexamer patterns. Experimentally, the racemic pattern； (c) was observed for HPF. The marroon crosses represent the structures are unfavoured.

Solvent can affect the self-assembly formation by changing molecular solubility, modulating surface mobility and adsorption stability, and thus induce the structural formation and transformation. At the solid–liquid interface, different polymorphisms can depend on the length of the alkyl chains of the solvent molecules due to the different solubility and adsorption capacity.[38] In the aliphatic solvents investigated, alkyl chain length of solvent dependence on the monolayer formation was observed. Fig. 14 (also see Table 1) displays that the value of S_m in *n*-hexadecane solvent, which is the unit cell area divided by the number of molecules per unit cell, is higher than other shorter aliphatic solvents at basically the same concentrations. Compared to the close-packed hexamer pattern in *n*-pentadecane under low concentrations, the value of S_m (2.3 nm^2 per molecule) for alternate pattern in *n*-hexadecane under low concentrations is slightly higher than that of the former (1.8 nm^2 per molecule), which reflects the loose-packed structures are in favor of formation for HPF molecules in longer chain aliphatic solvents. It should be noted that the racemic hexamer structure emerges in *n*-hexadecane and *n*-tetradecane solvents with even number of alkyl carbon atom under low concentrations, whereas that structure is not observed in *n*-pentadecane with odd number of alkyl carbon atom. That is, odd or even number of carbon–containing solvent molecules has induced extremely different nanostructures. The influence of this odd–even effect on the induced assembled structure can arise from the zigzag conformation of the alkyl chains.[39] Due to solvent coadsorption with the solute molecules, the influence of the underlying substrate lattice and steric repulsion forces, the odd or even number of alkyl carbon atom can modulate the direction of the end of methyl that lead to the formation of different structures in 2D self-assembly process.

In the molecular adsorption process onto the surface, different assembled structures of the HPF molecule could be observed in different solvents, especially during the inception stages of assembly. However, those structures would be eventually replaced by the zigzag structure, which was the thermodynamically most stable configuration, after being scanned for a short period of time. The dynamic transformation was observed through recording the STM images at the same location. Note that the transformation was monitored in a short time, so the effect of solvent evaporation could be neglected. As a consequence, we detect that the adsorption stability of the 2D self-assembled structures reduce when the alkyl chain length of solvent shortens. In addition, the rate of polymorphism transformation is likely to be more rapid in solvents with short chain (Fig. S11†). It is well-known that the 2D self-assembly structures at a liquid/solid interface involve a balance and competition between the molecule–molecule and molecule–substrate interactions. The adsorption of molecules from the solution onto the surface is under kinetic control. Owing to the decreased density of CH_2 units for the aliphatic solvent, the solvent–molecule vdWs interactions decrease. The number of molecules adsorbed from the solution on the surface per unit of area and time increases monotonically with the decrease of the chain length of solvents.[32] When the chain length of solvent decrease, the viscosity of solvent diminish. The decreased viscosity of the solution can expedite processing, which was the movement of molecules in and out of solution compared to that of solvent with long chain. Meantime, the solubility of HPF molecules would enhance with the decrease of the chain length of solvent, so that the denser zigzag structure was more favored to appear in *n*-dodecane due to a higher adsorption rate. In fact, the absorption energy for the solute molecules on the surface can be affected by the solvent. Since the alkyl chain length of coadsorbed solvent increases, the solvent–substrate interactions will strengthen. Therefore, the energy of HPF molecule in the solvent with long chain was expected to be larger than that of HPF molecule in the solvent with short chain. Consequently, the time absorbed on the surface would be longer for the HPF molecule in *n*-hexadecane solvent than in *n*-dodecane. These analyses would explain why the structural transition in *n*-tridecane and *n*-dodecane occurred in an exceedingly short time and hence high-resolution images of

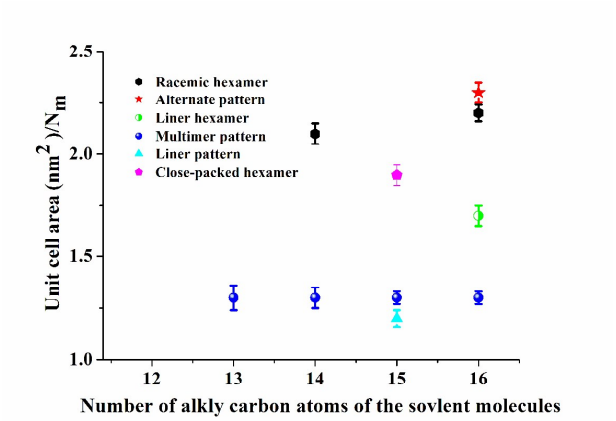

Fig. 14 Graph represents the evolution of S_m (unit cell area divided by the number of molecules per unit cell), on the basis of the nature of solvent and the alkyl chain length of solvent.

metastable structure could not be obtained in assembly process.

Meanwhile, due to steric matching and concentration effect, the closer the size of solvents to the alkoxy chain length of HPF, the easier the molecular arrangement exhibits the structural diversity. Fig. 14 displays that only the HPF molecule in *n*-hexadecane can form the most diversiform configurations. The adsorption energy of alkane-like molecules on graphite surface increases as the alkyl chain length increases.[40-41] Thus, increasing the alkyl chain length of coadsorbed solvent molecule can be in favor of the alkyl–graphite and the alkyl–alkyl chains vdWs interactions. In addition, the side chain length of HPF molecule is almost equal to that of *n*-hexadecane, which results in good structural size matching for the solvent molecules to coadsorb. This arrangement of coadsorption can maximize the molecule–solvent interactions.

Thermodynamic

At the solid–liquid interface, the surface coverage and stability of different self-assembled monolayers could dramatically depend both on solvent and solute concentration. Self-assembly was controlled by the balance of molecule–molecule, molecule–solvent, and solvent–substrate interactions. The assembly process is dynamic and depends on the adsorption–desorption equilibrium. To understand the effect of HPF concentration on the polymorphism in aliphatic solvent, the adsorption–desorption process under thermodynamic control was proposed. The adsorption–desorption equilibrium determined the surface coverage ratio of different structures. The concentration dependency of the self-assembly of HPF can therefore be understood as arising from the different stabilities and molecular densities of different polymorphs. Systematic concentration dependent experiments reveal that the changes in surface coverage of different self-assembled structures depend on the solution concentration in different kinds of aliphatic solvents (Fig. S12–S14†). Our results present a general observed trend for concentration induced self-assembled polymorphism at the solid–liquid interface: higher solution concentration leads to a more closer-packed arrangement (see Table 1). Because of the differences in dissolubility and adsorption capacity of these aliphatic solvents, the denser multimer pattern is easier to obtain at lower concentrations in aliphatic solvents with short chain. Meantime, the surface coverage ratio of the dense multimer pattern is also more sensitive towards the change of concentration in aliphatic solvents with short chain. Note that all structures would finally change into a zigzag structure. Assembled monolayer completely emerged from homogenous surface and no domain boundary was observed. In addition, the molecule–molecule and molecule–substrate vdWs interactions and intermolecular –OH···O= hydrogen bonds are so strong that all the conjugated moieties and the side chains lie in a line. These results indicate that the zigzag pattern is the most thermodynamically stable structure.

Conclusion

We have systematically studied the aliphatic solvent and concentration effects on the formation and transformation of chirality for the assembled structures of HPF molecule on HOPG surfaces. Because of the differences in dissolubility and adsorption capacity of these aliphatic solvents, the structural transition from chirality to nonchirality was pursued by tuning the concentration at the solid–liquid interfaces. Due to spatial matching and concentration effect, the HPF molecules with coadsorption of aliphatic solvent molecules formed several unique chiral structures *via* vdWs interactions at low concentrations, whereas the HPF molecules uniformly formed nonchiral dense multimer structure without coadsorbed solvent molecules at high concentrations. The distinct concentration–dependence has been proven that the aliphatic solvent can act as a coadsorbed component *via* vdWs interactions rather than simply dispersant and further result in its chiral formation probability and stability of the self-assembly monolayer by subtle tuning the solvent–molecule and solvent–substrate interactions. Finally, these structures will completely change into a zigzag structure, which is the thermodynamically most stable configuration. The results improve our understanding of aliphatic solvent effect on the formation of molecular chiral assembly, and fabrication and manipulation of chiral patterns at the solid–liquid interface.

Experimental Section

Details of the synthesis of 2-hydroxy-7-pentadecyloxy-9-fluorenone (HPF) molecules are reported according to a literature procedure.[29] Various solvents including *n*-hexadecane, *n*-pentadecane, *n*-tetradecane, *n*-tridecane and *n*-dodecane were purchased from TCI and used without further purification. To form assembly, about 2 µL solution that contained HPF molecule was dropped onto a freshly cleaved graphite surface (HOPG, quality ZYB; Bruker, USA), which was dissolved in aliphatic solvents with concentrations from 10^{-7} mol L^{-1} to 10^{-5} mol L^{-1} (molecular solubility of HPF in aliphatic solvents is poor). STM measurements were performed immediately using Nanoscope IIIa Multimode SPM (Bruker, USA) at the liquid/solid interface. STM experiments about the solution concentration dependence were carried out at

20–25 °C in the atmospheric environment. STM tips were prepared by mechanically cutting Pt/Ir wire (80:20). Except for flattening to remove the tilting effect of the substrate plane, the images were recorded under constant current mode and shown without further processing. The specific tunneling conditions are given in the captions. Different tips and samples were used to check the reproducibility of the results and exclude image artifacts that were caused by the tips or the samples. Molecular models of the observed assembled structures were constructed by using Materials Studio 4.4. The model of the monolayer was constructed by placing the molecules according to the intermolecular distances and angles that were obtained from analysis of the STM images. Molecular mechanics were applied for the structural optimization.

Acknowledgments

Financial supports from the National Program on Key Basic Research Project (2012CB932900, 2012CB619100), the National Natural Science Foundation of China (21103053, 51373055, 21403072, 51172073), the China Postdoctoral Science Foundation (2014M552189) and the Fundamental Research Funds for the Central Universities (SCUT) are gratefully acknowledged.

Notes and references

1. S. Weigelt, C. Busse, L. Petersen, E. Rauls, B. Hammer, K. V. Gothelf, F. Besenbacher and T. R. Linderoth, *Nat. Mater.,* 2006, **5,** 112–117.
2. L. Perez–Garcia and D. B. Amabilino, *Chem. Soc. Rev.*, 2007, **36,** 941–967.
3. K. H. Ernst, in Supramolecular Chirality, eds. M. Crego–Calama and D. Reinhoudt, Springer Berlin Heidelberg, 2006, vol. 265, ch. 36, pp. 209–252.
4. R. Fasel, M. Parschau and K.-H. Ernst, *Nature*, 2006, **439,** 449–452.
5. J. M. Bonello, F. J. Williams and R. M. Lambert, *J. Am. Chem. Soc.,* 2003, **125,** 2723–2729.
6. N. Katsonis, H. Xu, R. M. Haak, T. Kudernac, Ž. Tomović, S. George, M. Van der Auweraer, A. P. Schenning, E. e. W. Meijer and B. L. Feringa, *Angew. Chem. Int. Ed.,* 2008, **47,** 4997–5001.
7. A. Miura, P. Jonkheijm, S. De Feyter, A. P. H. J. Schenning, E. W. Meijer and F. C. De Schryver, *Small*, **2005,** 1, 131–137.
8. N. Katsonis, E. Lacaze and B. L. Feringa, *J. Mater. Chem.,* 2008, **18,** 2065–2073.
9. K. Tahara, H. Yamaga, E. Ghijsens, K. Inukai, J. Adisoejoso, M. O. Blunt, S. De Feyter and Y. Tobe, *Nat. Chem.,* 2011, **3,** 714–719.
10. Q. Chen, T. Chen, X. Zhang, L. J. Wan, H. B. Liu, Y. L. Li and P. Stang, *Chem. Commun.,* 2009, 3765–3767.
11. M. Ortega Lorenzo, C. J. Baddeley, C. Muryn and R. Raval, *Nature*, 2000, **404,** 376–379.
12. W. Mamdouh, H. Uji-i, A. E. Dulcey, V. Percec, S. De Feyter and F. C. De Schryver, *Langmuir*, 2004, **20**, 7678–7685.
13. D. Rohde, C. J. Yan, H. J. Yan and L. J. Wan, *Angew. Chem. Int. Edit,* 2006, **45,** 3996–4000.
14. A. M. Berg and D. L. Patrick, *Angew. Chem. Int. Ed.,* 2005, **44,** 1821–1823.
15. I. Destoop, E. Ghijsens, K. Katayama, K. Tahara, K. S. Mali, Y. Tobe and S. De Feyter, *J. Am. Chem. Soc.,* 2012, **134,** 19568–19571.
16. T. Chen, D. Wang, X. Zhang, Q. L. Zhou, R. B. Zhang and L. J. Wan, *J. Phys. Chem. C,* 2010, **114,** 533–538.
17. Y. L. Yang and C. Wang, *Curr. Opin. Colloid. In.,* 2009, **14,** 135–147.
18. T. Chen, W. H. Yang, D. Wang and L. J. Wan, *Nat. Commun.,* 2013, **4,** 1389.
19. C. J. Li, Q. D. Zeng, C. Wang, L. J. Wan, S. L. Xu, C. R. Wang and C. L. Bai, *J. Phys. Chem. B,* 2003, **107,** 747–750.
20. Z. X. Guo, I. De Cat, B. Van Averbeke, J. Lin, G. Wang, H. Xu, R. Lazzaroni, D. Beljonne, E. Meijer and A. P. Schenning, *J. Am. Chem. Soc.,* 2011, **133,** 17764–17771.
21. S. J. George, Ž. Tomović, A. P. Schenning and E. Meijer, *Chem Commun,* 2011, **47,** 3451–3453.
22. I. De Cat, Z. X. Guo, S. J. George, E. Meijer, A. P. Schenning and S. De Feyter, *J. Am. Chem. Soc.,* 2012, **134,** 3171–3177.
23. P. A. Korevaar, S. J. George, A. J. Markvoort, M. M. J. Smulders, P. A. J. Hilbers, A. P. H. J. Schenning, T. F. A. De Greef and E. W. Meijer, *Nature*, 2012, **481,** 492–U103
24. Q. Chen, T. Chen, D. Wang, H. B. Liu, Y. L. Li and L. J. Wan, *P. Natl. Acad. Sci.,* 2010, **107,** 2769–2774.
25. D. J. Lee, R. Cortini, A. P. Korte, E. L. Starostin, G. H. M. van der Heijden and A. A. Kornyshev, *Soft Matter,* 2013, **9,** 9833–9848.
26. T. Chen, W. H. Yang, D. Wang and L. J. Wan, *Nat. Commun.,* 2013, **4**, 1389.
27. L. Xu, X. R. Miao, B. Zha and W. L. Deng, *Chem.– Asia. J.,* 2013, **8,** 926–933.
28. L. Xu, X. R. Miao, B. Zha, K. Miao and W. Deng, *J. Phys. Chem. C*, 2013. **117,** 12707–12714.
29. L. Xu, X. R. Miao, X. Ying and W. L. Deng, *J. Phys. Chem. C,* 2011, **116,** 1061–1069.
30. L. Xu, X. R. Miao, B. Zha and W. L. Deng, *J. Phys. Chem. C,* 2012, **116,** 16014–16022.
31. B. Venkataraman, J. J. Breen and G. W. Flynn, *J. Phys. Chem.,* 1995, **99,** 6608–6619.
32. L. Kampschulte, M. Lackinger, A.-K. Maier, R. S. K. Kishore, S. Griessl, M. Schmittel and W. M. Heckl, *J. Phys. Chem. B,* 2006, **110,** 10829–10836.
33. K. Tahara, S. Furukawa, H. Uji-i, T. Uchino, T. Ichikawa, J. Zhang, W. Mamdouh, M. Sonoda, F. C. De Schryver, S. De Feyter and Y. Tobe, *J. Am. Chem. Soc.,* 2006, **128,** 16613–16625.
34. Y. T. Shen , N. Zhu, X. M. Zhang, K. Deng, W. Feng, Q. Yan, S. Lei, D. Zhao, Q.-D. Zeng and C. Wang, *Chem. – Eur. J.,* 2011, **17,** 7061–7068.
35. J. A. A. W. Elemans, I. De Cat, H. Xu and S. De Feyter, *Chem. Soc. Rev.,* 2009, **38,** 722–736.
36. M. Bohringer, K. Morgenstern, W. D. Schneider, R. Berndt, F. Mauri, A. De Vita and R. Car, *Phys. Rev. Lett.,* 1999, **83,** 324–327.
37. F. Vidal, E. Delvigne, S. Stepanow, N. Lin, J. V. Barth and K. Kern, *J. Am. Chem. Soc.*, 2005, **127,** 10101–10106.
38. M. Lackinger, S. Griessl, W. M. Heckl, M. Hietschold and G. W. Flynn, *Langmuir,* 2005, **21,** 4984–4988.
39. D. G. Yablon, D. Wintgens and G. W. Flynn, *J. Phys. Chem. B,* 2002, **106,** 5470–5475.

40. T. Müller, G. W. Flynn, A. T. Mathauser and A. V. Teplyakov, *Langmuir*, 2003, **19,** 2812–2821.
41. W. Mamdouh, H. Uji-i, J. S. Ladislaw, A. E. Dulcey, V. Percec, F. C. De Schryver and S. De Feyter, *J. Am. Chem. Soc.,* 2005, **128,** 317–325.